# EVIDENCE FOR INCREASED WAVINESS OF THE NORTHERN HEMISPHERE WINTERTIME POLAR AND SUBTROPICAL JETS

*by*

JONATHAN E. MARTIN

*Department of Atmospheric and Oceanic Sciences*
*University of Wisconsin-Madison*
*1225 W. Dayton St.*
*Madison, WI 53706*
608-262-9845
jemarti1@wisc.edu

Submitted for publication to *Journal of Climate*
August 15, 2018

ABSTRACT

A feature-based metric of the waviness of the wintertime [December-February (DJF)], Northern Hemisphere, tropopause-level polar and subtropical jets is developed and applied to the NCEP-NCAR reanalysis data. The analysis first identifies a “core isertel” along which the circulation per unit length is maximized in the separate polar (315:330 K) and subtropical (340:355 K) jet isentropic layers. Since the core isertel is, by design, an analytical proxy for the respective jet cores, calculation of its sinuosity is a robust measure of the waviness of the jets.

Analysis of the seasonal average waviness over a 66-year time series reveals that both jets have become systematically wavier while exhibiting no trends in their average speeds. Correlations of the daily sinuosities of the two jets suggest that the waviness of each evolves fairly independently of the other in most cold seasons. Finally, comparison of the composites of the waviest and least wavy seasons for each species reveals that interannual variability of the subtropical (polar) jet preferentially impacts Pacific (Atlantic) basin circulation anomalies in the troposphere. Meanwhile, in the lower stratosphere, wavy polar (subtropical) jet years are associated with an intensified (weakened) polar vortex.

## 1. Introduction

Among the most ubiquitous structural features of the Earth's atmosphere are the narrow, tropopause-level wind speed maxima known as jet streams or jets. These jets, often found nearly girdling the globe while exhibiting large meridional meanders, are the primary phenomena at the interface between synoptic-scale weather systems and the large-scale circulation. Consequently, they play a substantial role in the production of sensible weather in the mid-latitudes while serving as particularly influential governors of regional climate. Decades of observational work has identified two main varieties of jets, distinguished by their underlying dynamical origins. The polar jet (POLJ) forms as a result of eddy momentum flux convergence associated with the development of mid-latitude baroclinic waves (e.g. Held 1975; Rhines 1975; Panetta 1993) and is connected, via the thermal wind relationship, to the troposphere-deep baroclinicity of the middle latitudes. The subtropical jet (STJ) forms in response to angular momentum transport by the thermally direct Hadley circulation (Held and Hou 1980) and is, therefore, tied to the poleward edge of the tropical Hadley Cell. As a consequence of their different origins, the POLJ and STJ are often widely separated by latitude as well as elevation. The Northern Hemisphere (NH) jet stream has centers of maximum intensity located over the western Atlantic and western Pacific Oceans with the wintertime Pacific jet extending from East Asia to the date line. Unlike the Atlantic jet, the wintertime Pacific jet is regularly characterized by a collocation (or vertical superposition) of POLJ and STJ components and thus is often a hybrid feature (e.g. Christenson et al. 2017[1]).

Both species of jets reside near the tropopause – the thermodynamic boundary that

[1] Four times daily portrayals of the POLJ and STJ distributions in both the Northern and Southern Hemispheres, calculated using the 1° x 1° Global Forecast System (GFS) analyses from the National Center for Environmental Prediction (NCEP), are available at http://marrella.aos.wisc.edu/JET/jet.html

separates the stratosphere from the troposphere. The tropopause is characterized by strong first order discontinuities in static stability, the mixing ratios of certain chemical constituents, as well as potential vorticity (PV). Importantly, the tropopause does not occur at a uniform height over the entire hemisphere nor does it exhibit a monotonic slope with latitude. Instead, as first identified by Defant and Taba (1957), there is generally a three-step structure in tropopause height from pole-to-equator with local regions of steep slope occurring at successively lower elevation with increasing latitude.

These local maxima in slope are also regions of large PV gradient on isentropic surfaces. This PV gradient serves as the restoring force for Rossby waves, the ubiquitous, planetary-scale ridge-trough couplets that are primarily responsible for the production of organized weather systems in the extratropics. Morgan and Nielsen-Gammon (1998) demonstrated the utility of maps of $\theta$ and wind speed on the so-called dynamic tropopause (defined as a surface of constant Ertel (1942) PV) for diagnosing weather systems. In this framework, the maxima in tropopause slope become regions of large PV gradient on isentropic surfaces, or large $\theta$ gradient on isertelic (constant PV) surfaces, and are theoretically (Cunningham and Keyser 2004) and empirically (Davies and Rossa 2008) linked to the tropopause-level jet cores.

The behavior of the jets in a warmer climate has been a topic of considerable research effort recently. The consensus view is that a robust poleward displacement of the jet axes will likely characterize a warmer world (e.g. Yin 2005, Miller et al. 2006, Swart and Fyfe 2012, Woollings and Blackburn 2012, Barnes and Polvani 2013). In addition, attempts have been made, by various methods, to assess the waviness of the mid-latitude flow containing the jets. Particularly at issue in recent years has been attribution of any such changes to the enhanced lower tropospheric warming at high latitudes known as Arctic amplification (Serreze et al. 2009, Screen and Simmonds 2010). Nearly all such attempts have employed analysis metrics involving geopotential height contours or horizontal wind components in the middle and upper troposphere (e.g. Francis and Vavrus 2012 and 2015, Barnes 2013, DiCapua and Coumou 2016). However, considered from a PV perspective, the flow at 500 hPa is often strongly influenced by lower boundary thermal contrasts (i.e. low-level PV gradients following Bretherton (1966)) and internal diabatic processes as well as PV anomalies at the tropopause (Hoskins et al. 1985, Davis and Emanuel 1991). Thus, though the 500 hPa flow often exhibits similarities to the jet stream flows at higher altitudes, because it is shaped by these lower tropospheric and diabatic influences to a greater extent than the tropopause-level flow, it might be expected that tropopause-level jet waviness would differ noticeably from that of the mid-troposphere. Consistent with this presumption and, despite a number of recent innovations in objective identification of the jet streams themselves (e.g. Schiemann et al. 2009, Manney et al. 2011, Limbach et al. 2012, Christenson et al. 2017), agreement on whether or not substantial changes in jet waviness have been detected does not yet exist (Barnes and Screen, 2015). Underlying this lack of consensus is the absence of a robust method of assessing the waviness of the tropopause-level jets. Without regard to the question of possible links to Arctic amplification, the goals of the present paper are limited to describing a method for separately quantifying the waviness of the subtropical and polar jets, examining recent trends in both, and considering aspects of the hemispheric circulation anomalies associated with extremes in waviness of both species.

The paper is organized as follows. A theoretical and observational background to the methodology used in the study is given in Section 2 along with a description of the data set used. In Section 3 aspects of the long-term trend and interannual variability of the waviness of the Northern Hemisphere, cold-season subtropical and polar jets are considered. Included here are analyses of the differences in the composite, large-scale dynamic and kinematic structures associated with the waviest and least-wavy cold seasons in both species of tropopause-level jets. A summary and conclusions, including suggestions for future work, are offered in Section 4.

## 2. Data and Methodology

In this study, the waviness of the two species of tropopause-level jets is assessed in the context of understanding their relationships to the gradient of PV in prescribed isentropic layers. Christenson et al. (2017) presented an objective method for identification of the separate polar and subtropical jets in θ/PV space. They argued that the Northern Hemisphere cold season (NDJFM) polar (subtropical) jet core lies on the equatorward, or low PV, edge of a strong PV gradient in the 315:330 K (340:355K) isentropic layer.[2] Justification for the PV gradient/jet relationship follows from consideration of the quasi-geostrophic potential vorticity (QGPV) following Cunningham and Keyser (1994). Recalling that QGPV is given by

$$q_g = \frac{1}{f_o}\nabla^2\phi + f + \frac{\partial}{\partial p}\left(\frac{f_o}{\sigma}\frac{\partial\phi}{\partial p}\right) = \Lambda(\phi) + f$$

(where $\Lambda = \frac{1}{f_o}\nabla^2 + \frac{\partial}{\partial p}\left(\frac{f_o}{\sigma}\right)\frac{\partial}{\partial p} + \frac{f_o}{\sigma}\frac{\partial^2}{\partial p^2}$ and $f$ is the geopotential), the cross-jet gradient of QGPV ($\frac{\partial q_g}{\partial n}$ where $\hat{n}$ is the cross-flow direction in natural coordinates) can be expressed as

$$\frac{\partial q_g}{\partial n} = \Lambda\left(\frac{\partial\phi}{\partial n}\right) = \Lambda(-fV_g) \qquad (1)$$

after substituting from the natural coordinate expression for the geostrophic wind. Thus, local maxima in the cross-flow gradient of QGPV are collocated with maxima in the geostrophic wind

[2] The threshold value is $0.64 \times 10^{-5}$ PVU $m^{-1}$ ($0.64 \times 10^{-11}$ m K $kg^{-1}$ $s^{-1}$) for both the 315:330 and 340:355 K layers.

speed. The analysis of Davies and Rossa (1998) offers empirical justification for confident extension of this relationship to gradients in Ertel (1942) PV.

In the foregoing analysis we employ the zonal (*u)* and meridional (*v)* winds as well as temperature (*T)* from 66 winters (DJF) of National Centers for Environmental Prediction (NCEP) – National Center for Atmospheric Research (NCAR) reanalysis data, at 6-h intervals, spanning the period 1 December 1948 to 28 February 2014. The NCEP-NCAR reanalysis data are available at 17 isobaric levels (1000, 925, 850, 700, 600, 500, 400, 300, 250, 200, 150, 100, 70, 50 , 30, 20, and 10 hPa) with a 2.5° latitude-longitude grid spacing (Kalnay et al. 1996; Kistler et al. 2001). These data were bilinearly interpolated onto isentropic surfaces at 5-K intervals from 300 to 370 K using programs within the General Meteorology Package (GEMPAK) (desJardins et al. 1991). The average PV and average zonal and meridional wind speeds in both the polar (315:330 K) and subtropical (340:355K) layers were then calculated four times daily for every day in the 66 year time series.

By virtue of the fact that the jets are always located in a region of strong PV gradient, a reasonable proxy for the axis of maximum wind speed (or "core") of each jet is, on any given day, one of several isertels within the strong gradient region. We shall refer to this particular isertel as the "core isertel" and note here that it need not have the same value from one day to the next. We seek to quantify the daily departure from zonality of such core isertels in each jet layer as a means of directly assessing the waviness of the jet. In order to perform this analysis, we first consider the circulation

$$C = \oint \vec{U} \cdot d\vec{l}$$

along isertels ranging from 0.5 to 5.0 PVU (at 0.1 PVU intervals, 1 PVU = $10^{-6}$ $m^2$ K $kg^{-1}$ $s^{-1}$ ) in each jet layer on every day in the time series. The core isertel in each layer on a given day is the isertel along which the average $\vec{U}$ per unit length is maximized. Randomly selected examples illustrating the utility of this method for identifying the meandering cores of the subtropical and the polar jets are provided in Figs. 1 and 2, respectively. Note that the "stray" jet core in Fig. 1d, an isolated wind speed maxima far removed from the core isertel in the subtropical (340:355 K) layer, is actually the vertical extension of an obvious polar jet in the underlying 315:330 K layer (Fig. 2d). Conversely, the "stray" wind speed maxima over the Middle East and the Himalaya in Fig. 2d is the lower portion of the subtropical jet core, identified in the 340:355 K layer (Fig. 1d). Throughout the time series, a large fraction of such seemingly disconnected isotach maxima in either layer can be accounted for in a similar fashion.

As stated earlier, the core isertel is not the same for each day in the time series and thus its distribution in each jet layer is worthy of additional analysis. Figure 3 portrays the cumulative distribution functions for the core isertels of both the subtropical and polar jets.[3] More than 6 of every 7 DJF days had a core isertel in the STJ layer between 1 and 3 PVU with a mode of 2.0 PVU (Fig. 3a). The polar jet distribution is shifted toward lower PV values (Fig. 3b) consistent with the concept of a "dynamically relevant PV contour" as described by Kunz et al. (2015). The mode of 1.2 PVU represents nearly 1 in 6 days all by itself while nearly 80% of all DJF days have a polar jet core isertel between 1 and 3 PVU.

Once the core isertel for a given day has been identified, we consider its sinuosity. Sinuosity is a simple, commonly used metric in fluvial geomorphology that measures the meanders of rivers and streams by calculating the ratio of the length of a segment of a stream to the length of the shortest distance between the endpoints of the segment (Leopold et al. 1964). A schematic example is given in Fig. 4. Sinuosity has only recently been introduced into the

[3] The distribution of core isertel for the subtropical jet has become wider and flatter throughout the time series as revealed by a comparison of the two 30 years periods from 1950-1979 and 1980-2009. No such difference arose from a similar comparison of distributions for the polar jet.

meteorological literature (Cattiaux et al. 2016, Vavrus et al. 2017) following an unpublished note by Martin et al. (2016). The extension of this idea employed in the present study follows from considering the core isertel as a proxy for the jet axis in a given isentropic layer. The waviness of the respective jet is then assessed by determining the sinuosity of the core isertel in that layer – a process that begins by calculating the area enclosed by it. Next, an equivalent latitude[4] is computed for that isertel - defined as the latitude poleward of which the area is equal to the area enclosed by the core isertel. Finally, the sinuosity is defined as the ratio of the length of the core isertel to the circumference of its equivalent latitude circle. It follows from this definition that the values of sinuosity are constrained to be greater than or equal to 1.0 where that minimum value describes a purely zonal jet with no waviness. As an example, the sinuosities of the tropopause-level jets observed on 18 February 1998 were 1.200 for the STJ (Fig. 1d) and 1.449 for the POLJ (Fig. 2d).

## 3. Analysis

*a. Seasonal averages*

The seasonal average sinuosity of each jet is calculated as a simple 90-day (no leap days) average of the daily sinuosity in each cold season. The results of this averaging are shown in Fig. 5 and it is immediately apparent that the polar jet is substantially wavier than its subtropical counterpart. Though characterized by considerable interannual variability, both jets exhibit an increase in seasonally averaged waviness over the 66 winters, significant at the 99.9% level. For

[4] If A is the area enclosed by the core isertel at a given time, then the equivalent latitude, $\phi_e$, is given by $\phi_e = \arcsin[1 - \frac{A}{2\pi R_e^{\,2}}]$, where $R_e$ is the radius of the Earth.

comparison, we also calculated the aggregate sinuosity of the 500 hPa geostrophic flow using 5 isohypses ranging from 576 to 528 dm (at 120 m intervals) chosen because they contain the maximum 500 hPa geostrophic wind throughout the cold season. The aggregate sinuosity is the ratio of the sum of the lengths of these 5 isohypses divided by the sum of the circumferences of their equivalent latitude circles. As seen in Fig. 5, employment of isohypses at 500 hPa as a means of assessing the waviness of the mid-latitude flow, as has recently been suggested by a number of studies (e.g. Francis and Vavrus 2012, Barnes 2013, Screen and Simmonds 2014, Overland et al, 2015, DiCapua and Coumou 2016), does not similarly testify to an increase in jet waviness.

Daily time series of the sinuosity of each jet in a single cold season can also be constructed and compared to one another, as shown, for example, in Fig. 6 for the winter of 1990/91. Diagnosing the large- and synoptic-scale processes responsible for the day-to-day evolution of each jet's waviness is beyond the scope of the present work. Of interest instead is whether or not, and to what extent, the waviness of the two jets varies together. For the example season of 1990/91 the correlation between the two time series is quite low (r=0.1969). In fact, the lack of even a modest correlation between the waviness of the two jets in a given cold season appears to be the rule rather than the exception. In 35 of the 66 winters in the time series, the two are correlated with magnitudes less than 0.2 with 19 of those winters exhibiting correlations with magnitudes less than 0.1. Only 10 of the 66 cold seasons had correlations with magnitudes exceeding 0.3, three exceeded 0.4, with only two of them over 0.5[5]. Thus, despite synoptic evidence of episodic periods of substantial and impactful interaction between them (e.g. Uccellini et al. 1984, Bosart et al. 1996, Winters and Martin 2014), it appears that throughout an

[5] These two winters were 1967-68 and 1982-83.

average NH cold season the waviness of the two jet species evolves with a fair degree of independence.

The analysis also reveals that the seasonal average circulation along the core isertel in each jet layer has been increasing[6] (Fig. 7a). Interestingly, however, there is no trend in the corresponding average $U$ for either jet (Fig. 7b). These two results, coupled with the systematic increase in the waviness of the jets illustrated in Fig. 5, demonstrate that a wavier jet does not necessarily imply a weaker jet.

*b. Impact of variability in jet waviness on Northern Hemisphere wintertime circulation*

Using the daily time series from each season, such as that in Fig. 6, it is possible to identify the waviest and least wavy seasons for each jet species by simply summing the daily departures from average over the 90 days of each cold season. The list of integrated seasonal departures from average waviness for each species is shown in Table 1. From this list, four highly ranked seasons in each waviness category for a given jet were identified that simultaneously exhibited nearly average waviness in the other species. As an example, the waviest POLJ seasons also characterized by minimal perturbation STJ waviness were 1992-93, 1991-92, 1990-91, and 1975-76 which ranked first, third, fourth and fifth, respectively, on the list of wavy POLJ seasons. The least wavy POLJ seasons meeting the constraint of minimal perturbation STJ waviness were 1966-67, 1981-82, 1970-71, and 1985-86 which ranked fourth, eighth, ninth, and twelfth, respectively, on the list of least wavy POLJ seasons. These chosen four from each category of POLJ seasons were all at or above the 87th percentile for their

[6] These trends are also significant at the 99.9% level.

categories. Similar choices for the extremes in STJ waviness resulted in selections that were at or above the $80^{th}$ percentile of all STJ seasons[7].

This selection process was motivated by a desire to examine the influence of relatively "pure" extremes of a single jet species on elements of the wintertime hemispheric circulation through comparison of composites. Composites of several variables from the waviest and least wavy POLJ and STJ seasons thus selected were constructed. In the subsequent analysis we show differences in each variable obtained by subtracting the least wavy from the waviest composite.

Figure 8a shows the 500 hPa geopotential height differences between seasons with the waviest and least wavy polar jets. Wavy polar jet seasons are attended by height anomalies reminiscent of the positive North Atlantic Oscillation (NAO) in the north Atlantic (Fig. 8a). The height differences that exist between extremes of waviness of the subtropical jet are much more focused in the Pacific basin where anomalous ridging centered on the Gulf of Alaska extends from the west coast of North America to the dateline (Fig. 8b).

Related to these middle tropospheric height differences are differences in the 300 hPa zonal wind. In the north Atlantic the wavy polar jet seasons are characterized by a poleward displacement of the jet axis and a weakening of the zonal wind in a band stretching across the basin from near the northeastern United States to Iberia and the Mediterranean. In the Pacific basin, wavy polar jet years appear to have little influence on the Pacific jet along nearly the length of its climatological axis (Fig. 9a). The influence of subtropical jet variability on the circulation changes in the north Atlantic is weaker and displaced westward (Fig. 9b). In the Pacific basin wavy subtropical jet seasons encourage a poleward displacement of the jet over the

[7] The waviest STJ seasons meeting the selection criteria were 1999-00, 2012-13, 1993-94, and 1984-85 which ranked sixth, ninth, eleventh, and twentieth of all STJ seasons. The least wavy STJ seasons were 1957-58, 1961-62, 1994-95 and 1979-80 which ranked fifth, ninth, seventeenth, and eighteenth among all STJ seasons.

Bering Sea and Gulf of Alaska and a broadly weaker flow equatorward of the climatological jet position in the central Pacific. Such a distribution of anomalies is similar to that associated with north Pacific jet retractions (Jaffe et. al 2011) which represent one phase of the leading mode of jet variability in the basin (Athanasiadis et al. 2010).

The geographic concentration of the signals associated with extremes in POLJ and STJ waviness suggested in Figs. 8 and 9 is made more obvious in composite differences in 1000 hPa geopotential heights (Fig. 10). The polar jet extremes are clearly connected to an NAO-type signal (Fig. 10a) while anomalous ridging in the Gulf of Alaska (and the Arctic) characterizes the STJ differences (Fig. 10b).[8]

The circulation differences engendered by the inter-seasonal variability in jet waviness are apparently not confined to the troposphere. Associated modulations to the lower stratospheric polar vortex are illustrated in Fig. 11. Wavy polar jet years are associated with a greatly intensified polar vortex rung by light height rises at middle latitudes (Fig. 11a). Lower stratospheric circulation changes arising from inter-seasonal variation in the waviness of the subtropical jet have nearly the exact opposite polarity (Fig. 11b) which may have implications for the likelihood of sudden stratospheric warmings in a given season as well as for the nature and timing of the final warming.

## 4. Summary

The analysis presented here focuses on observed morphlogical aspects of the Northern Hemisphere tropopause-level jet streams during boreal winter (DJF) over the last six and a half

[8] The correlation between the time series of seasonal average sinuosity and the NAO index (from the Climate Prediction Center (available at http://www.cpc.ncep.noaa.gov/products/precip/CWlink/pna/norm.nao.monthly.b5001.current.ascii.table) is 0.482 for the STJ and 0.492 for the POLJ.

decades. Based upon the definitions of the polar and subtropical jets offered by Christensen et al. (2017), the analysis identifies a "core isertel" along which the circulation per unit length is maximized in the separate polar (315:330K) and subtropical (340:355K) isentropic layers for each day in the 66-year time series. Such a core isertel represents an analytical proxy for the respective jet cores. Calculation of the sinuosity of the core isertel is, therefore, a robust, feature-based metric of the waviness of each species of jet. The analysis reveals that both jets are becoming systematically wavier while exhibiting no trends in their average speeds. Interannual variability of the subtropical (polar) jet appears to preferentially impact the Pacific (Atlantic) basin circulation anomalies as revealed by a comparison of composites of the waviest minus least wavy seasons of each species.

In their examination of long term changes in the amplitude of 500 hPa waves, Screen and Simmonds (2013) spectrally decomposed isohypse patterns into their different wave number contributions and then assessed changes in the amplitudes of the various wave numbers. An intriguing prospect for future work would be to perform a spectral decomposition of the core isertels to gain insight into the physical structures and processes that underlie the increase in jet waviness. The core isertels, however, especially for the polar jet, are rather frequently folded over themselves along longitude lines. While this morphology has no effect on the identification of the core isertels or calculations of their sinuosity, it does render straightforward application of a Fourier analysis to the daily data impossible. Temporal averaging of the winds and PV in each jet layer may prove effective in overcoming this issue but at the cost of unwanted filtering of synoptic short waves. Resolution of this analysis problem is deferred to subsequent work.

The same folding over of isertels that impedes spectral analysis lies at the heart of another issue inspired by these results; namely, the interactive nature of increased waviness and poleward migration of the jets. A number of prior investigators (e.g. Thorncroft et al. 1993; Benedict et al. 2004; Rivière and Orlanski 2007; Martius et al. 2007; Strong and Magnusdottir 2008; Woollings et al. 2008; Rivière 2009) have examined the poleward momemtum flux characteristic of certain configurations of the large scale flow. These analyses have concluded that individual synoptic-scale eddies can play an important role in the formation of large-scale flow anomalies through wave breaking. Vallis and Gerber (2008) have suggested that high impact teleconnections such as the North Atlantic Oscillation (NAO), the Pacific North America pattern (PNA) and the annular modes are fundamentally related to fluctuations in the latitude and amplitude of the tropopause-level jets. Introduction of the LC1/LC2 life cycle dichotomy by Thorncroft et al. (1993) represented a recognition that anticyclonic (LC1) and cyclonic (LC2) wave breaking lay at the heart of the interaction of eddies with the larger scale flow. When anticyclonic wave breaking occurs near the jet core, the jet is pushed poleward in response to the associated distribution of momentum fluxes. Framed in terms of the PV gradient, Rivière (2009) concluded that a higher latitude jet is more likely to experience anticyclonic wavebreaks which would, in turn, encourage further poleward displacement. If the increased waviness reported here has been manifest as an increase in the frequency of positively tilted waves, then the attendant poleward migration of the jets may bear a direct dynamical link to the waviness. Examination of this potential connection, dependent on construction of an objective method for identifying the tilt of the waves, following the work of Wernli and Sprenger (2007) and Martius et al. (2008), is a subject of ongoing research.

Equally unknown in the wake of the present analysis is the precise role of the tropics in forcing the observed increased waviness of the subtropical jet. A recent analysis of the subtropical jet by Martius (2014) considered the interaction of the tropics and extratropics with the jet from the perspective of trajectory analysis. She showed that air parcels that ended up in the jet over Africa (East Asia/western Pacific) ascended over South America (Indian Ocean and the Maritime Continent) before following an anticyclonic path toward the jet. The analysis showed that the wintertime Hadley circulation is zonally asymmetric connecting tropical convection in localized regions to segments of the jet. Whether or not the increased waviness of the subtropical jet is directly related to changes in such tropical convective forcing is not known though a recent analysis by Röthlisberger et. al (2018) suggests a connection. In order to gain some sense of a relationship we counted the number of days in a cold season with standardized daily waviness greater than 1.5 and calculated its correlation with the Mean ENSO Index (MEI) for the season. The two measures were entirely uncorrelated (r = -0.009, not shown). Possible connections between other modes of organized tropical convection (such as the MJO) and the trend in subtropical jet waviness are yet to be explored.

In their analysis of the major stratospheric sudden warming (SSW) of January 2006, Coy et al. (2009) identified a precursor lower stratospheric subtropical wavebreaking event in the north Atlantic. They showed that the poleward heat flux associated with a developing 200 hPa ridge forced a change in the stratospheric polar vortex that led sequentially to the wavebreak and the warming. Martius et al. (2009) showed that nearly all SSWs identified in the ERA-40 data set were preceded by blocks, best identified at 200 hPa. Common to both analyses is their dependence on highly amplified 200 hPa flow which is consistent with a wavy STJ. Cross-referencing the climatology of Charlton and Polvani (2007) with Table 1 indicates that only half of the seasons that experienced a SSW were also characterized by an anomalously wavy STJ[9].

[9] Only 10 of the 18 SSW seasons had greater than average POLJ waviness though in 13 of them the perturbation waviness of the two jets was of the same sign.

Thus, though wavy STJ seasons encourage a slightly weakened polar vortex (Fig. 11b), such seasons do not appear to have a direct impact on the likelihood of a SSW.

Finally, the analysis methodology introduced here has been applied hemispherically but could equally be employed in regional analyses. Such a regional analysis of the 500 hPa flow over North America and its relation to Arctic amplification and hemispheric snow cover was recently performed by Vavrus et al. (2017). A primary motivation for shrinking the analysis domain was their suspicion that doing so would enhance the strength of the desired signal. Indeed, DiCapua and Coumou (2016) found that regional trends in their meandering index were 2 to 3 times larger than those observed over the full hemisphere. It is anticipated that separate application of the present analysis method to the Atlantic and Pacific basins will add additional insight into the regional preferences already suggested by the composite difference fields shown in Figs. 8-11. We hope to pursue such applications in future work.

## REFERENCES


Athanasiadis, P. J., J. M. Wallace, and J. J. Wettstein, 2010: Patterns of wintertime jet stream variability and their relation to the storm tracks. *J. Atmos. Sci.*, **67**, 1361–1381.

Barnes, E. A., 2013: Revisiting the evidence linking Arctic amplification to extreme weather in midlatitudes. *Geophys. Res. Let.*, **40**, 4734-4739.

_____, and L. Polvani, 2013: Response of the midlatitude jets, and of their variability, to increased greenhouse gases in the CMIP5 models. *J. Climate*, **26**, 7117-7135.

_____, and J. A. Screen, 2015: The impact of Arctic warming on the midlatitude jet-stream: Can it? Has it? Will it? *WIREs Clim Change*, **6**, 277–286. doi: 10.1002/wcc.337.

Benedict, J., S. Lee, and S. Feldstein, 2004: Synoptic view of the North Atlantic Oscillation. *J. Atmos. Sci*., **61**, 121–144.

Bosart, L. F., G. J. Hakim, K. R. Tyle, M. A. Bedrick, W. E. Bracken, M. J. Dickinson, and D. M. Schultz, 1996: Large-scale antecedent conditions associated with the 12–14 March 1993 cyclone ("Superstorm '93") over eastern North America. *Mon. Wea. Rev*., **124**, 1865-1891.

Bretherton, F. P., 1966: Critical layer instability in baroclinic flows. *Quart. J. Royal Meteor. Soc.*, **92**, 325–334.

Cattiaux, J., Y. Peings, D. Saint-Martin, N. Trou-Kechout, and S. J. Vavrus, 2016: Sinuosity of midlatitude atmospheric flow in a warming world. *Geophys. Res. Let.*, **43**, 8259–8268, doi: 10.1002/2016GL070309.

Charlton, A. J., and L. M. Polvani, 2007: A new look at stratospheric sudden warmings. Part I: Climatology and modeling benchmarks. *J. Climate*, **20**, 449-469.

Christenson, C. E., J. E. Martin, and Z. J. Handlos, 2017: A synoptic-climatology of Northern Hemisphere, cold season polar and subtropical jet superposition events. *J. Climate*, **30**, 7231-7246.

Coy, L., S. Eckermann, and K. Hoppel, 2009: Planetary wave breaking and tropospheric forcing as seen in the stratospheric sudden warming of 2006. *J. Atmos. Sci*., **66**, 495-507.

Cunningham, P., and D. Keyser, 2004: Dynamics of jet streaks in a stratified quasi-geostrophic atmosphere: Steady-state representations. *Quart. J. Roy. Meteor. Soc.,* **130,** 1579-1609.

Davies, H. C., and A. M. Rossa, 1998: PV frontogenesis and upper-tropospheric fronts. *Mon. Wea. Rev.*, **126**, 1528-1539.

Davis, C. A., and K. A. Emanuel, 1991: Potential vorticity diagnostics of cyclogenesis.

*Mon. Wea. Rev.*, **119**, 1929–1953

Defant, F., and H. Taba, 1957: The threefold structure of the atmosphere and the characteristics of the tropopause. *Tellus*, **9**, 259-275.

desJardins, M. L., K. F. Brill, and S. S. Schotz, 1991: Use of GEMPAK on UNIX workstations. Preprints, *Seventh Int. Conf. on Interactive Information and Processing Systems for Meteorology, Oceanography, and Hydrology*, New Orleans, LA, Amer. Meteor. Soc., 449–453.

DiCapua G., and D. Coumou,2016: Changes in the meandering of the Northern Hemisphere circulation. *Environ. Res. Lett.*, **11**, 094028, doi:10.1088/1748-9326/11/9/094028.

Ertel, H., 1942: Ein Neuer hydrodynamischer Wirbelsatz. *Meteor. Z.*, **59**, 271-281.

Francis, J. A., and S. J. Vavrus, 2012: Evidence linking Arctic amplification to extreme weather in mid-latitudes. *Geophys. Res. Let.*, **39**, L06801, doi:10.1029/2012GL051000.

_____, and _____, 2015: Evidence for a wavier jet stream in response to rapid Arctic warming. *Environ. Res. Lett.* **10**, 014005, doi:10.1088/1748-9326/10/1/014005.

Held, I. M., 1975: Momentum transport by quasi-geostrophic eddies. *J. Atmos. Sci.*, **32**, 1494-1497.

____, and A. Y. Hou, 1980: Nonlinear axially symmetric circulations in a nearly inviscid atmosphere. *J. Atmos. Sci*., **37**, 515-533.

Hoskins, B. J., M. E. McIntyre, and A. W. Robertson, 1985: On the use and significance of isentropic potential vorticity maps. *Quart. J. Roy. Meteor. Soc*., **111**, 877–946.

Jaffe, S. C., J. E. Martin, D. J. Vimont and D. J. Lorenz, 2011: A synoptic climatology of episodic, subseasonal retractions of the Pacific jet. *J. Climate*, **24**, 2846–2860.

Kalnay, E. and co-authors, 1996: The NCEP/NCAR 40-year reanalysis project. *Bull. Amer. Meteor. Soc*., **77**, 437-470.

Kistler, R. and co-authors, 2001: The NCEP-NCAR 50-Year reanalysis: Monthly means CD-ROM and documentation. *Bull. Amer. Meteor. Soc*., **82**, 247-267.

Kunz, A., M. Sprenger, and H. Wernli, 2015: Climatology of potential vorticity streamers and associated isentropic transport pathways across PV gradient barriers, *J. Geophys. Res. Atmos*., **120**, 3802–3821, doi:10.1002/2014JD022615.

Leopold. L. B., M. G. Wolman, and J. Miller, 1964: *Fluvial processes in geomorphology*. W. H. Freeman & Co., San Francisco, 522 p.

Limbach, S., Schömer, E., and Wernli, H.: Detection, tracking and event localization of jet stream features in 4-D atmospheric data, *Geosci. Model Dev.*, **5**, 457-470.

Manney, G. L., Hegglin, M. I., Daffer, W. H., Santee, M. L., Ray, E. A., Pawson, S., Schwartz, M. J., Boone, C. D., Froidevaux, L., Livesey, N. J., Read, W. G., and Walker, K. A.: Jet characterization in the upper troposphere/lower stratosphere (UTLS): Applications to climatology and transport studies. *Atmos. Chem. Phys.*, **11**, 6115–6137, doi:10.5194/acp-11-6115-2011.

Martin, J. E., S. J. Vavrus, F. Wang, and J. A. Francis, 2016: Sinuosity as a measure of middle tropospheric waviness. (available at http://marrella.aos.wisc.edu/Martin.html).

Martius, O., 2014: A Lagrangian analysis of the Northern Hemisphere subtropical jet. *J. Atmos. Sci.*, **71**, 2354-2369.

_____, C. Schwierz, and H. Davies, 2007: Breaking waves at the tropopause in the wintertime Northern Hemisphere: Climatological analyses of the orientation and the theoretical LC1/2 classification. *J. Atmos. Sci.*, **64**, 2576–2592.

_____, C. Scwierz, and H. C. Davies, 2008: Far-upstream precursors of heavy precipitation on the Alpine south-side. *Quart. J. Roy. Meteor. Soc.*, **134**, 417-428.

_____, L. M. Polvani, and H. C. Davies, 2009: Blocking precursors to stratospheric sudden warming events. *Geophys. Res. Let.*, **36**, L14806, doi:10.1029/2009GL038776.

Miller, R. L., G. A. Schmidt, and D. T. Shindell, 2006: Forced annular variations in the 20th century Intergovernmental Panel on Climate Change Fourth Assessment Report models. *J. Geophys. Res.*, **111**, D18101, doi:10.1029/2005JD006323.

Morgan, M. C., and J. W. Nielsen-Gammon, 1998: Using tropopause maps to diagnose midlatitude weather systems. *Mon. Wea. Rev.*, **126**, 2555-2579.

Overland, J., J. A. Francis, R. Hall, E. Hanna, S-J Kim, and T. Vihma, 2015: The melting Arctic and midlatitude weather patterns: Are they connected? *J. Climate*, **28**, 7917-7932.

Panetta, R. L., 1993: Zonal jets in wide baroclinically unstable regions: Persistence and scale selection. *J. Atmos. Sci.*, **50**, 2073-2106.

Rhines, P. B., 1975: Waves and turbulence on a beta-plane. *J. Fluid Mech.*, **69**, 417-443.

Rivière, G., 2009: Effect of latitudinal variations in low-level baroclinicity on eddy life cycles and upper-tropospheric wave-breaking processes. *J. Atmos. Sci.*, **66**, 1569-1592.

_____, and I. Orlanski, 2007: Characteristics of the Atlantic storm-track eddy activity and its relation with the North Atlantic Oscillation. *J. Atmos. Sci.*, **64**, 241–266.

Röthlisberger, M., O. Martius, and H. Wernli, 2018: Northern Hemisphere Rossby wave initiation events on the extratropical jet – a climatological analysis. *J. Climate*, **31**, 743-760.

Scheimann, R., D. Lüthi, and C. Schär, 2009: Seasonality and interannual variability of the westerly jet in the Tibetan Plateau region. *J. Climate*, **22**, 2940-2957.

Screen, J. A., and I. Simmonds, 2010: The central role of diminishing sea ice in recent Arctic temperature amplification. *Nature*, **464**, 1334-1337.

____, and _____, 2013: Exploring links between Arctic amplification and mid-latitude weather. *Geophys. Res. Let.*, **40**, 959-964.

_____, and _____, 2014: Amplified mid-latitude planetary waves favour particular regional weather extremes. *Nature Climate Change*, **4**, 704-709.

Serreze, M. C., A. P. Barrett, J. C. Stroeve, D. N.  Kindig, and M. M. Holland, 2009: The emergence of surface-based Arctic amplification, *The Cryosphere*, **3**, 11-19.

Strong, C., and G. Magnusdottir, 2008: Tropospheric Rossby wave breaking and the NAO/NAM. *J. Atmos. Sci.*, **65**, 2861–2876.

Swart, N. C., and J. C. Fyfe, 2012: Observed and simulated changes in the Southern Hemisphere surface westerly wind-stress. *Geophys. Res. Let.*, **39**, L16711, doi:10.1029/2012GL052810.

Thorncroft, C. D., B. J. Hoskins, and M. McIntyre, 1993: Two paradigms of baroclinic-wave life-cycle behaviour. *Quart. J. Roy. Meteor. Soc.*, **119**, 17–55.

Uccellini, L. W., P. J. Kocin, and R. A. Petersen, 1984: The Presidents' Day cyclone of 18–19 February 1979: Synoptic overview and analysis of the subtropical jet streak influencing the pre-cyclogenetic period. *Mon. Wea. Rev.*, **112**, 31-55.

Vallis, G. K., and E. P. Gerber, 2008: Local and hemispheric dynamics of the North Atlantic Oscillation, annular patterns and the zonal index. *Dyn. Atmos. and Oceans*, **44**, 184-212.

Vavrus, S. J., F. Wang, J. E. Martin, J. A. Francis, Y. Peings, and J. Cattiaux, 2017: Changes in North American circulation and extreme weather: Influence of arctic amplification and Northern Hemisphere snow cover. *J. Climate* , **30**, 4317-4333.

Wernli, H. and Sprenger, 2007: Identification and ERA-15 climatology of potential vorticity streamers and cutoffs near the extratropical tropopause. *J. Atmos. Sci.*, **64**, 1569-1586.

Winters, A. C., and J. E. Martin, 2014: The role of a polar/subtropical jet superposition in the May 2010 Nashville Flood. *Wea. Forecasting*, **29**, 954-974.

Woollings, T. and M. Blackburn, 2012: The north Atlantic jet stream under climate change and its relation to the NAO and EA patterns. *J. Climate*, **25**, 886-902.

Woollings, T., B. Hoskins, M. Blackburn, and P. Berrisford, 2008: A new Rossby wave–breaking interpretation of the North Atlantic oscillation. *J. Atmos. Sci.*, **65**, 609–626.

Yin, J. H., 2005: A consistent poleward shift of the storm tracks in simulations of 21$^{st}$ century climate. *Geophys. Res. Let.*, **32**, L18701,doi:10.1029/2005GL023684.

| ***YEAR*** | *POLJ* | *STJ* | ***YEAR*** | *POLJ* | *STJ* |
|---|---|---|---|---|---|
| ***1948*** | -1.065 | -0.670 | ***1981*** | -7.156 | 0.549 |
| ***1949*** | -3.482 | -2.904 | ***1982*** | 1.908 | -1.097 |
| ***1950*** | -4.362 | -3.690 | ***1983*** | -2.398 | -0.242 |
| ***1951*** | -0.502 | 0.093 | ***1984*** | 0.873 | 1.785 |
| ***1952*** | -5.247 | -2.382 | ***1985*** | -5.018 | 0.175 |
| ***1953*** | -4.513 | -2.605 | ***1986*** | 1.925 | 1.487 |
| ***1954*** | -3.286 | -1.255 | ***1987*** | 0.396 | 1.459 |
| ***1955*** | -4.513 | -2.880 | ***1988*** | 6.903 | 7.327 |
| ***1956*** | -5.045 | -2.263 | ***1989*** | 5.907 | 4.603 |
| ***1957*** | -0.642 | -4.511 | ***1990*** | 8.386 | 0.099 |
| ***1958*** | 2.376 | -0.870 | ***1991*** | 10.630 | -1.034 |
| ***1959*** | -4.563 | -1.902 | ***1992*** | 14.835 | 0.712 |
| ***1960*** | -2.782 | -1.388 | ***1993*** | -1.223 | 3.856 |
| ***1961*** | 0.398 | -3.793 | ***1994*** | 0.352 | -2.749 |
| ***1962*** | -3.206 | -5.131 | ***1995*** | -3.333 | -1.313 |
| ***1963*** | -9.171 | -4.761 | ***1996*** | 2.748 | 5.059 |
| ***1964*** | 3.092 | 2.103 | ***1997*** | 2.289 | -3.894 |
| ***1965*** | -7.488 | -3.574 | ***1998*** | 6.765 | 4.785 |
| ***1966*** | -7.957 | -0.145 | ***1999*** | 1.640 | 4.838 |
| ***1967*** | -3.306 | -3.551 | ***2000*** | -3.975 | 2.692 |
| ***1968*** | -9.438 | -6.027 | ***2001*** | 5.243 | 4.108 |
| ***1969*** | -9.337 | -4.368 | ***2002*** | -2.942 | -0.506 |
| ***1970*** | -6.946 | -0.928 | ***2003*** | 3.695 | 1.893 |
| ***1971*** | -4.659 | 1.047 | ***2004*** | 7.141 | -3.356 |
| ***1972*** | 2.256 | -3.795 | ***2005*** | 2.493 | 2.510 |
| ***1973*** | -1.977 | 3.025 | ***2006*** | 6.223 | 1.579 |
| ***1974*** | -4.651 | 2.619 | ***2007*** | 5.023 | 5.904 |
| ***1975*** | 8.194 | -0.267 | ***2008*** | 7.714 | 7.380 |
| ***1976*** | -4.512 | -2.013 | ***2009*** | -3.356 | -4.988 |
| ***1977*** | -7.685 | -3.294 | ***2010*** | 11.176 | 2.023 |
| ***1978*** | 0.224 | 1.453 | ***2011*** | 3.268 | 3.720 |
| ***1979*** | 0.791 | -2.672 | ***2012*** | 0.079 | 4.211 |
| ***1980*** | 7.303 | -0.579 | ***2013*** | 7.489 | 8.306 |

**Table 1** Integrated seasonal departure from average waviness for polar (*POLJ*) and subtropical (*STJ*) jets for each year in the time series. The indicated year for each season includes December.

## FIGURE CAPTIONS

**Fig. 1** Isotachs of the daily average wind speed (contoured every 10 m $s^{-1}$ and shaded above 30 m $s^{-1}$) and the core isertel (bold solid line) in the 340:355 K isentropic layer on (a) 19 January 1958, (b) 26 December 1968, (c) 19 February 1979, and (d) 18 February 1998. The core isertel has a value of 2.0 PVU in (a), 2.1 PVU in (b), 2.1 PVU in (c), and 1.4 PVU in (d). Blue dashed line in (d) represents a portion of the axis of the polar jet on the same day in the 315:330 K isentropic layer (see Fig. 2d and text for explanation).

**Fig. 2** Isotachs of the daily average wind speed (contoured every 10 m $s^{-1}$ and shaded above 30 m $s^{-1}$) and the core isertel (bold solid line) in the 315:330 K isentropic layer on (a) 12 December 1954, (b) 8 January 1967, (c) 6 February 1978, and (d) 18 February 1998. The core isertel value is 1.6 PVU in (a), 1.0 PVU in (b), 1.8 PVU in (c), and 2.2 PVU in (d). Red dashed line in (d) represents a portion of the axis of the subtropical jet on the same day in the 340:355 K isentropic layer (see Fig. 1d and text for explanation).

**Fig. 3** Cumulative distribution of core isertel value for the 66-season time series in (a) the 340:355 K layer and (b) the 315:330 K layer. Isertel values given in potential vorticity units (PVU, 1 PVU = $10^{-6}$ K $m^2$ $kg^{-1}$ $s^{-1}$).

**Fig. 4** Schematic illustrating the concept of sinuosity. $\boldsymbol{S_{AB}}$ is the ratio of the length of the blue contour to the length of the red line segment AB.

**Fig. 5** Seasonal average sinuosity of the NH wintertime subtropical (solid red line) and polar (solid blue line) jets for each cold season from 1948-49 to 2013-14. The thin black line through each time series represents the trend line for each and is significant at the 99.9% level. Dashed gray line is the seasonal average aggregate sinuosity of the 500 hPa geostrophic flow between 528 and 576 dm (see text for explanation). The "YEAR" on the abscissa indicates the year in which December of that cold season occurred.

**Fig. 6** Times series of daily sinuosity of the polar (blue line) and subtropical (red line) jets for the cold season 1990-91. The correlation between the two time series is given at the bottom right.

**Fig. 7** (a) Seasonal average circulation along the core isertel for the subtropical (solid red line) and polar (solid blue line) jets. The thin black line through each time series is the trend line which is significant at the 99.9% level. (b) Seasonal average ***U*** along the core isertel for the subtropical (red solid line) and polar (blue solid line) jets.

**Fig. 8** 500 hPa height differences between composite waviest and least wavy (a) polar jet and (b) subtropical jet seasons. See text for explanation and identification of the specific years comprising each composite. Positive (negative) height differences are in solid (dashed) lines, labeled in m and contoured every 20m (-20m) beginning at 20m (-20m).

**Fig. 9** 300 hPa zonal wind differences between composite waviest and least wavy (a) polar jet and (b) subtropical jet seasons. See text for explanation and identification of the specific years comprising each composite. Positive (negative) wind differences are in solid (dashed) lines, labeled in $m\ s^{-1}$ and contoured every $5\ m\ s^{-1}$ ($-5\ m\ s^{-1}$) beginning at $5\ m\ s^{-1}$ ($-5\ m\ s^{-1}$). Red solid lines represent climatological axes of the DJF 300 hPa zonal wind.

**Fig. 10** 1000 hPa height differences between composite waviest and least wavy (a) polar jet and (b) subtropical jet seasons. See text for explanation and identification of the specific years comprising each composite. Positive (negative) height differences are in solid (dashed) lines, labeled in m and contoured every 8m (-8m) beginning at 8m (-8m).

**Fig. 11** 50 hPa height differences between composite waviest and least wavy (a) polar jet and (b) subtropical jet seasons. See text for explanation and identification of the specific years comprising each composite. Positive (negative) height differences are in solid (dashed) lines, labeled in m and contoured every 20m (-20m) beginning at 20m (-20m).

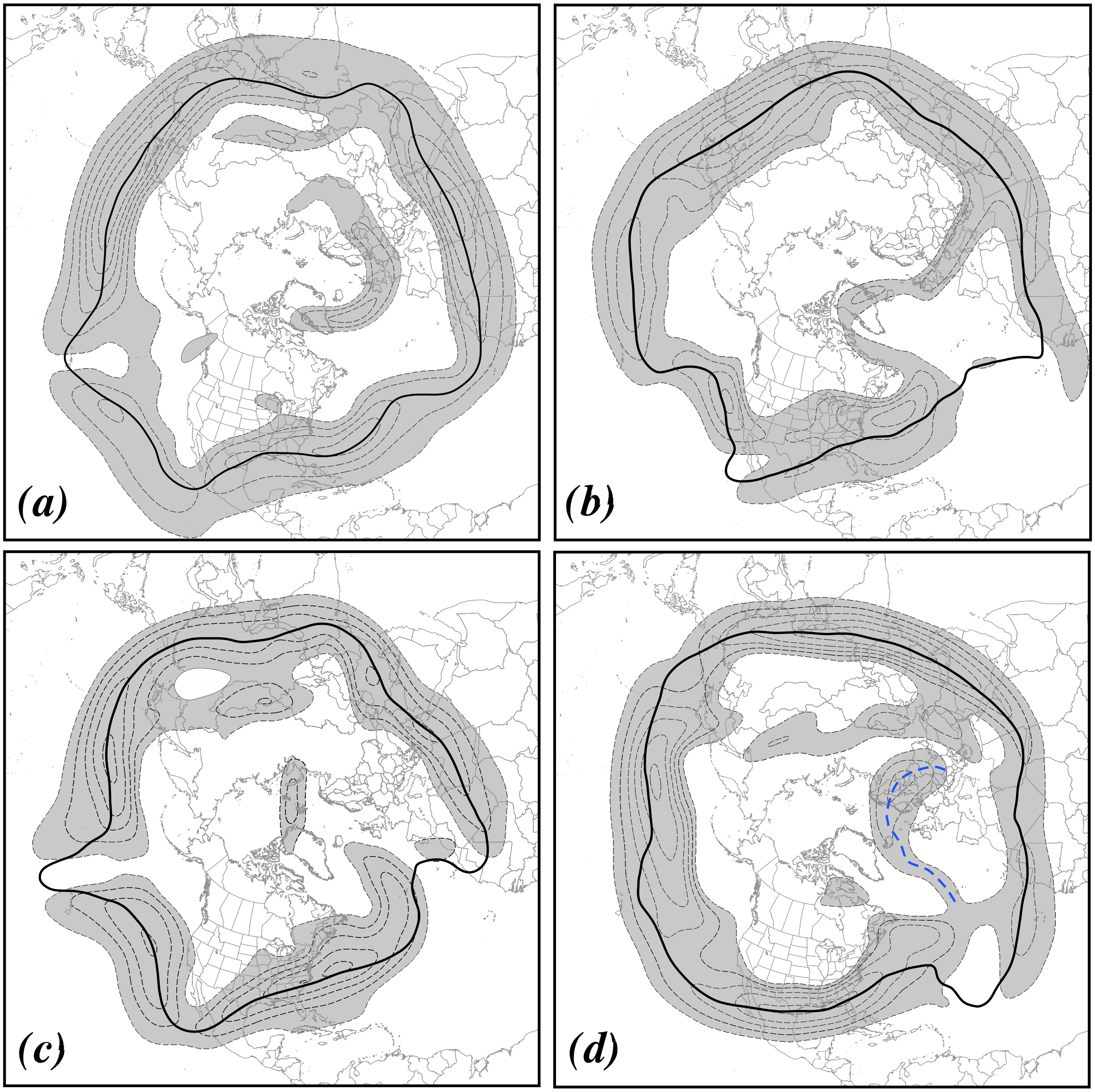


Fig. 1 Isotachs of the daily average wind speed (contoured every 10 m $s^{-1}$ and shaded above 30 m $s^{-1}$) and the core isertel (bold solid line) in the 340:355 K isentropic layer on (a) 19 January 1958, (b) 26 December 1968, (c) 19 February 1979, and (d) 18 February 1998. The core isertel has a value of 2.0 PVU in (a), 2.1 PVU in (b), 2.1 PVU in (c), and 1.4 PVU in (d). Blue dashed line in (d) represents a portion of the axis of the polar jet on the same day in the 315:330 K isentropic layer (see Fig. 2d and text for explanation).

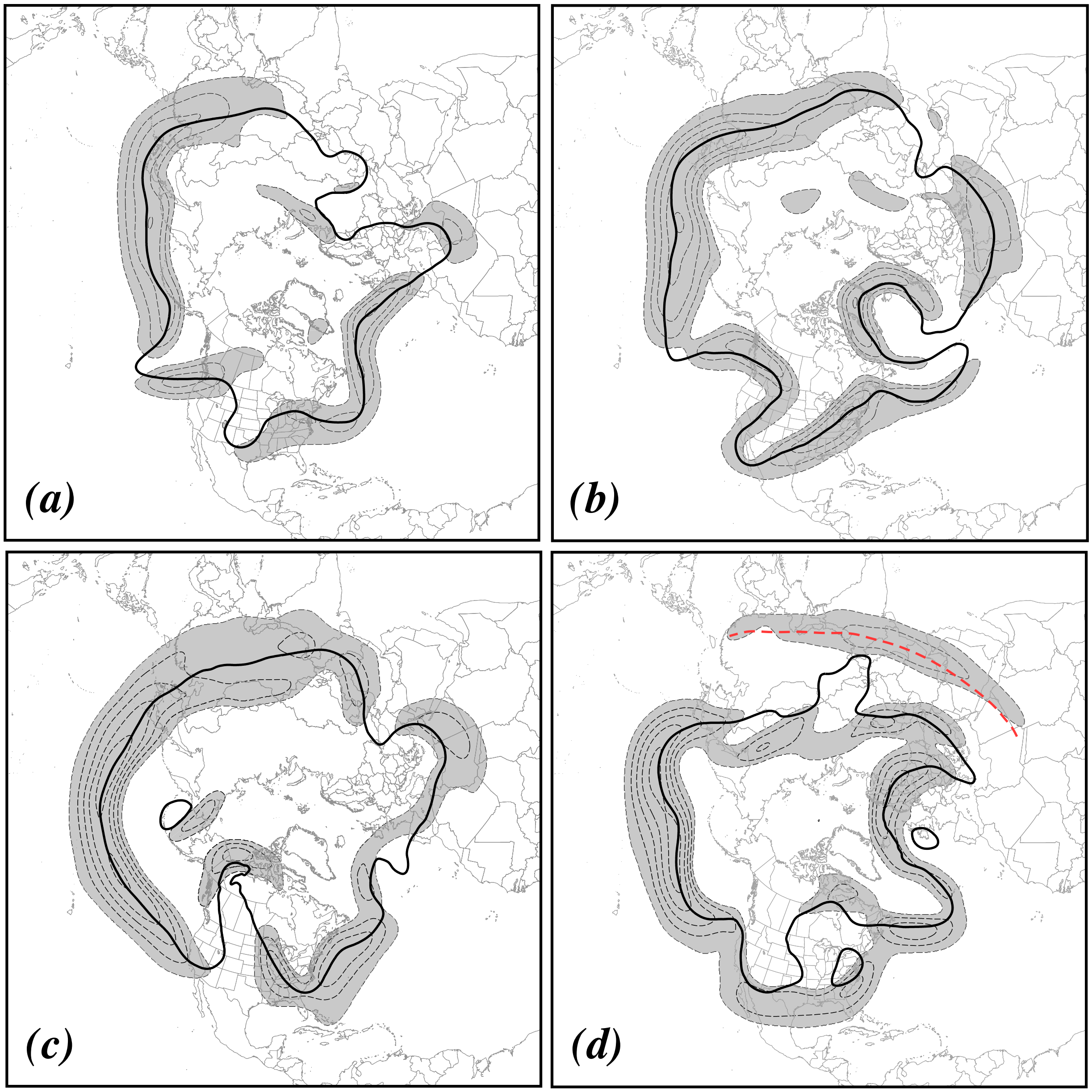


Fig. 2 Isotachs of the daily average wind speed (contoured every 10 m $s^{-1}$ and shaded above 30 m $s^{-1}$) and the core isertel (bold solid line) in the 315:330 K isentropic layer on (a) 12 December 1954, (b) 8 January 1967, (c) 6 February 1978, and (d) 18 February 1998. The core isertel value is 1.6 PVU in (a), 1.0 PVU in (b), 1.8 PVU in (c), and 2.2 PVU in (d). Red dashed line in (d) represents a portion of the axis of the subtropical jet on the same day in the 340:355 K isentropic layer (see Fig. 1d and text for explanation).

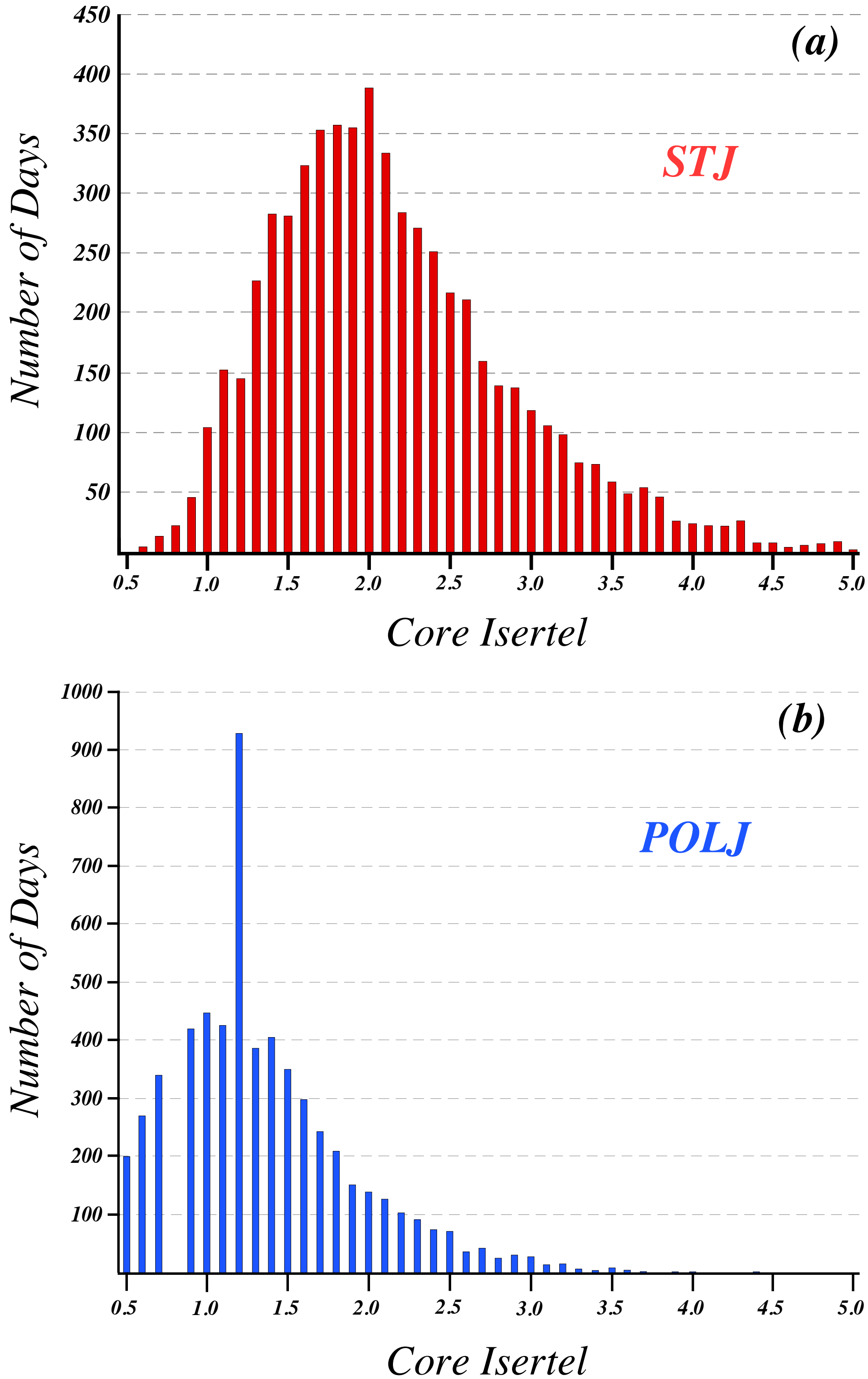


Fig. 3. Cumulative distribution of core isertel value for the 66-season time series in (a) the 340:355 K layer and (b) the 315:330 K layer. Isertel values given in potential vorticity units (PVU, 1 PVU = $10^{-6}$ K $m^2$ $kg^{-1}$ $s^{-1}$).

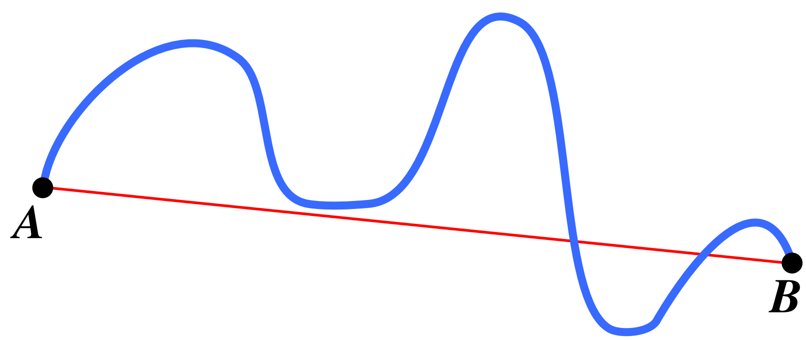


$$S_{AB} = \frac{\text{(Length of CONTOUR)}}{\text{(Length of SEGMENT)}}$$

Fig. 4 Schematic illustrating the concept of sinuosity. $S_{AB}$ is the ratio of the length of the blue contour to the length of the red line segment AB.

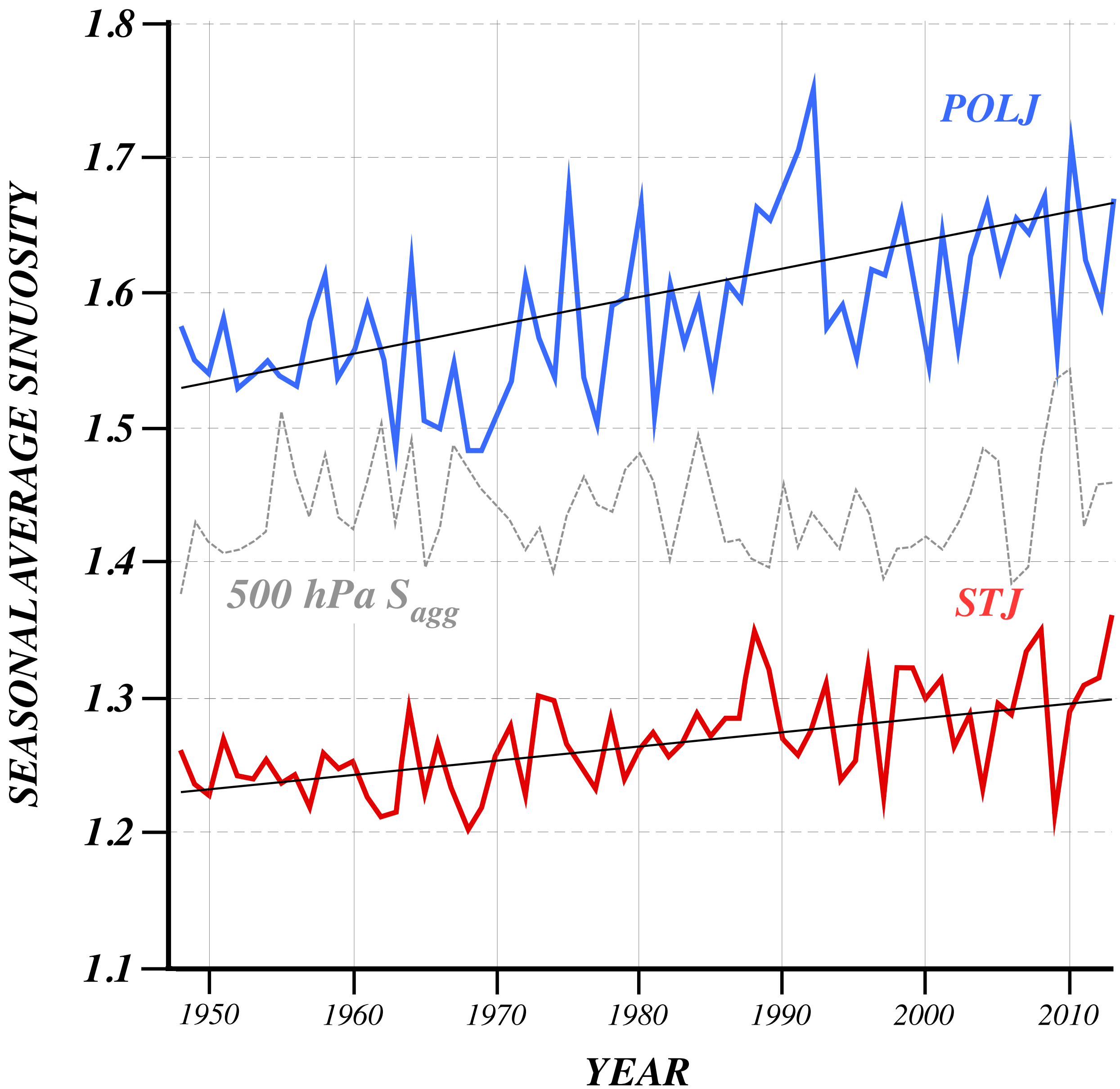


Fig. 5 Seasonal average sinuosity of the NH wintertime subtropical (solid red line) and polar (solid blue line) jets for each cold season from 1948-49 to 2013-14. The thin black line through each time series represents the trend line for each and is significant at the 99.9% level. Dashed gray line is the seasonal average aggregate sinuosity of the 500 hPa geostrophic flow between 528 and 576 dm (see text for explanation). The "YEAR" on the abscissa indicates the year in which December of that cold season occurred.

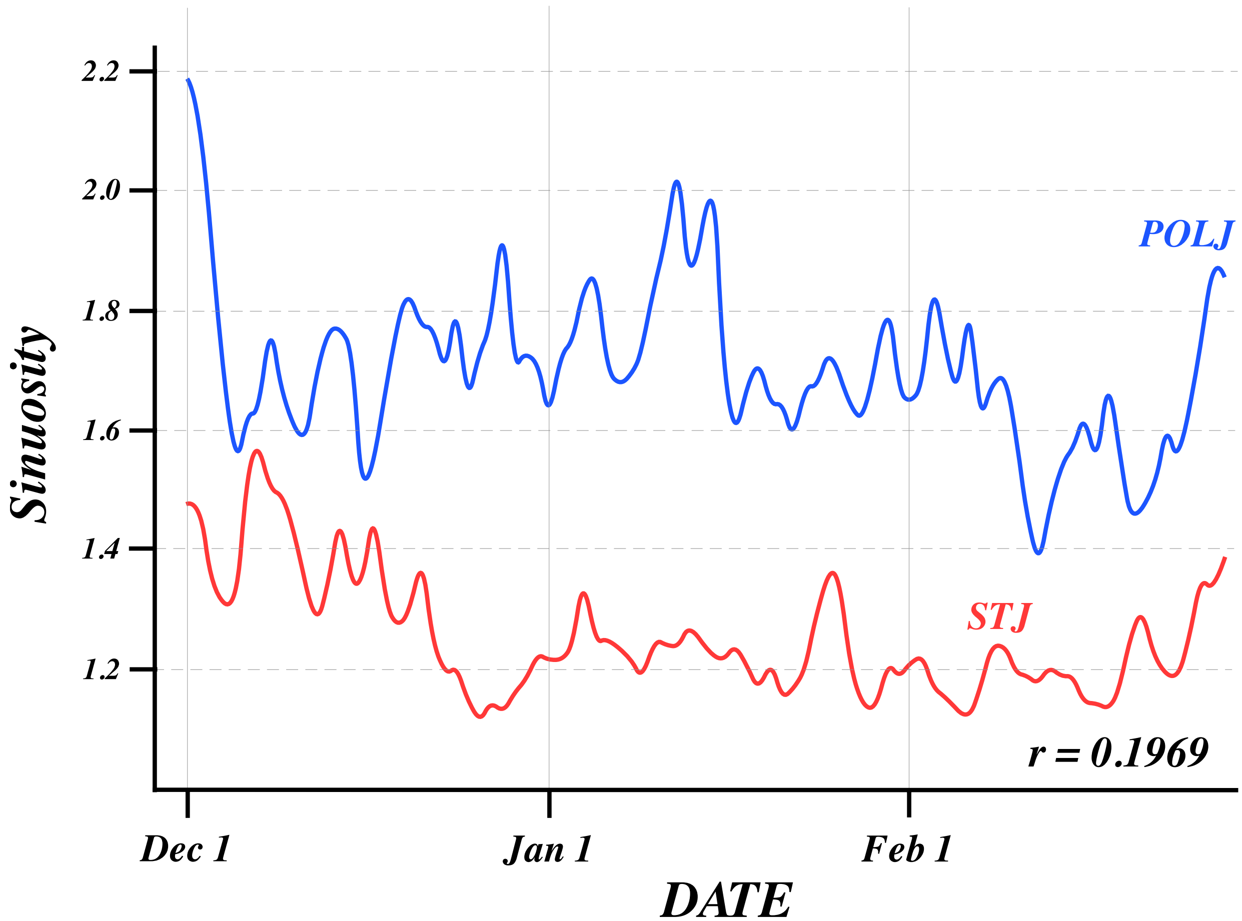


Fig. 6 Times series of daily sinuosity of the polar (blue line) and subtropical (red line) jets for the cold season 1990-91. The correlation between the two time series is given
636 at the bottom right.

637

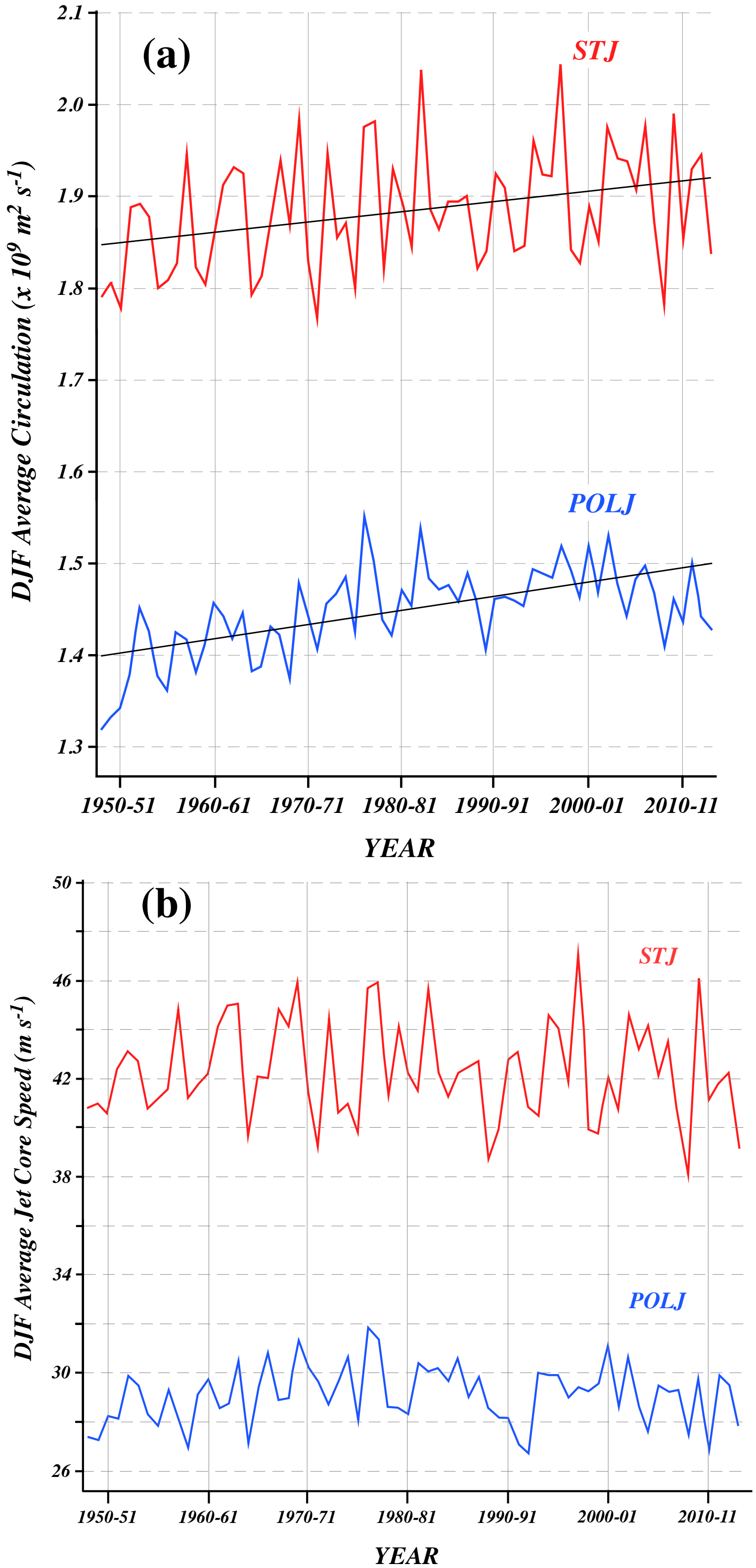


Fig. 7 (a) Seasonal average circulation along the core isertel for the subtropical (solid red line) and polar (solid blue line) jets. The thin black line through each time series is the trend line which is significant at the 99.9% level. (b) Seasonal average ***U*** along the core isertel for the subtropical (red solid line) and polar (blue solid line) jets.

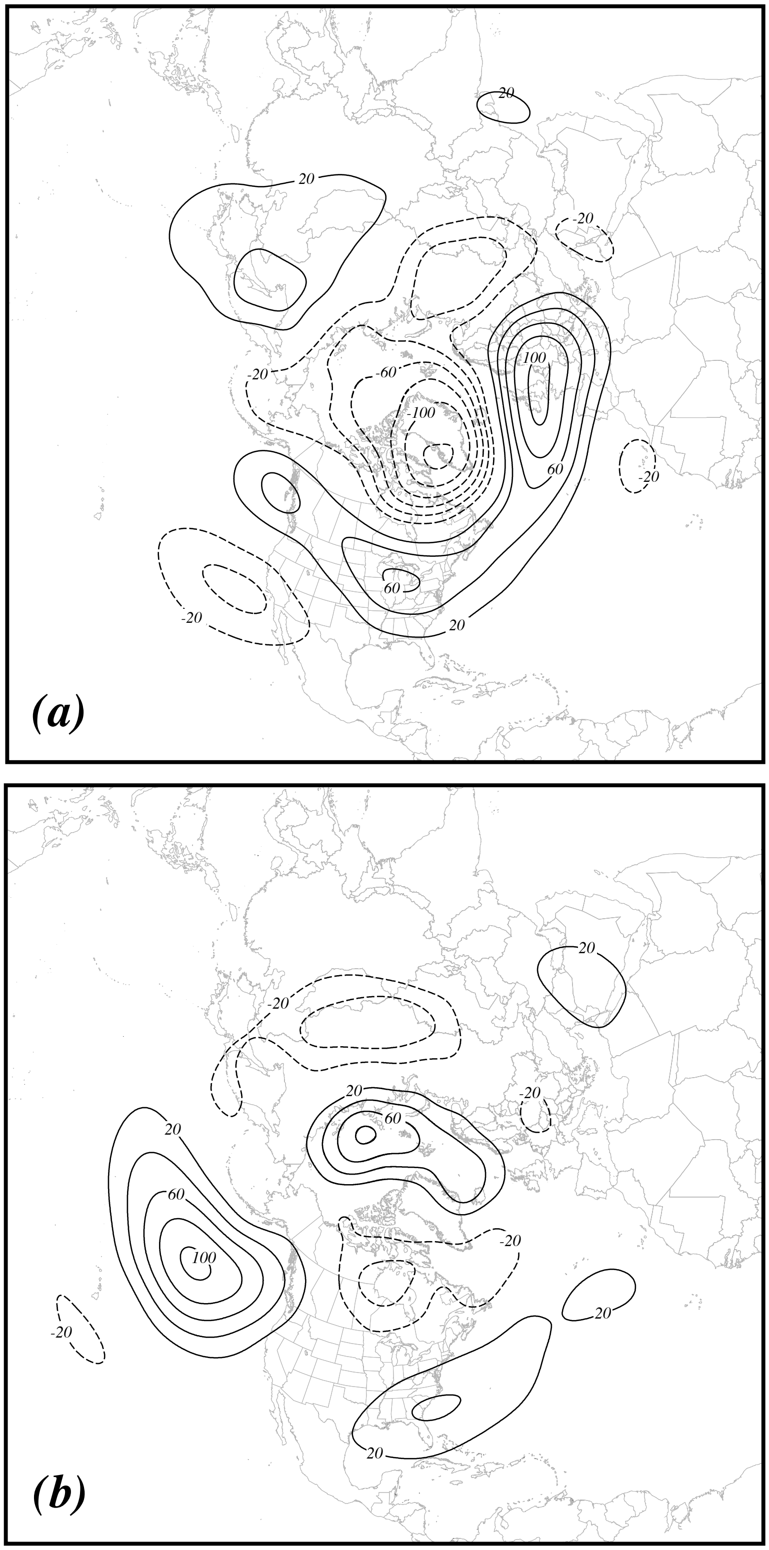


Fig. 8. 500 hPa height differences between composite waviest and least wavy (a) polar jet and (b) subtropical jet seasons. See text for explanation and identification of the specific years comprising each composite. Positive (negative) height differences are in solid (dashed) lines, labeled in m and contoured every 20m (-20m) beginning at 20m (-20m).

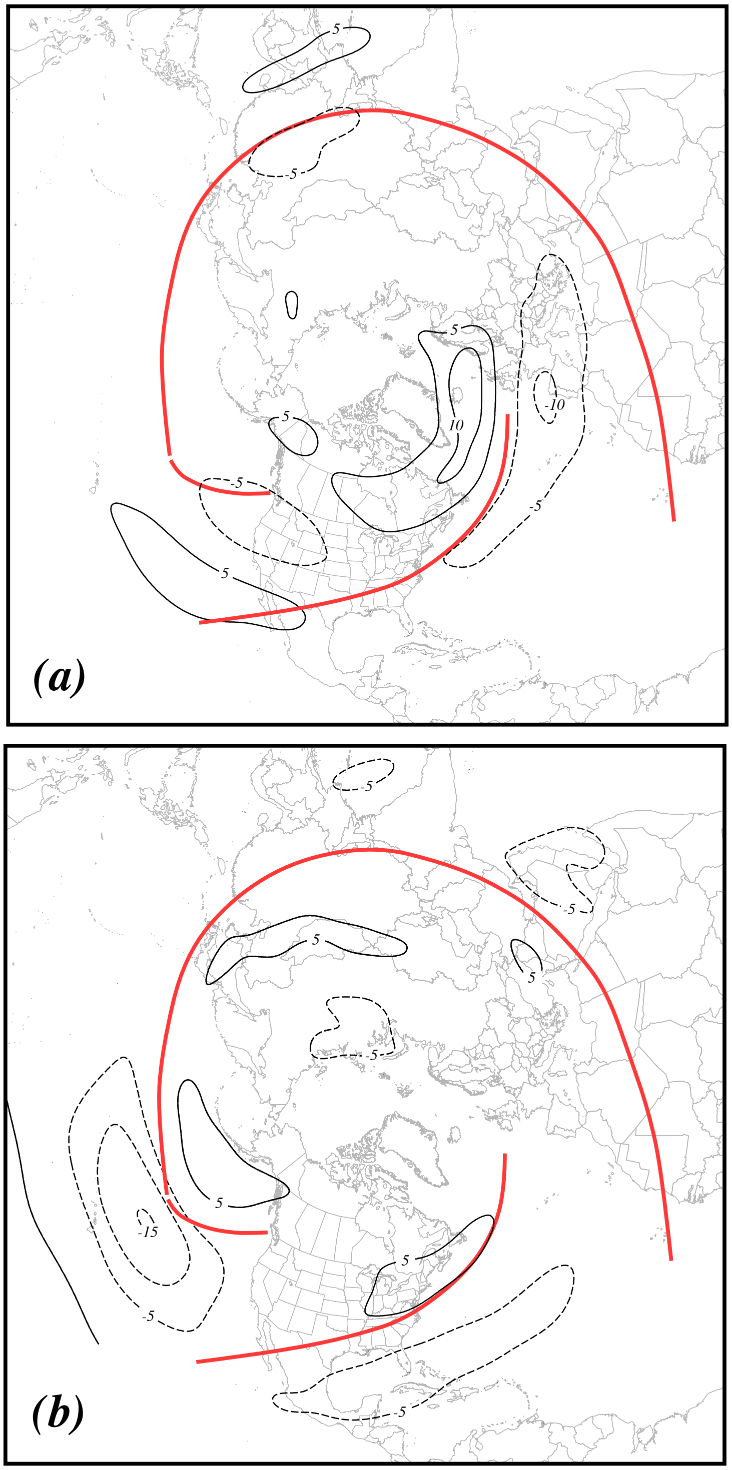


Fig. 9. 300 hPa zonal wind differences between composite waviest and least wavy (a) polar jet and (b) subtropical jet seasons. See text for explanation and identification of the specific years comprising each composite. Positive (negative) wind differences are in solid (dashed) lines, labeled in m $s^{-1}$ and contoured every 5 m $s^{-1}$ (-5 m $s^{-1}$) beginning at 5 m $s^{-1}$ (-5 m $s^{-1}$). Red solid lines represent climatological axes of the DJF 300 hPa zonal wind.

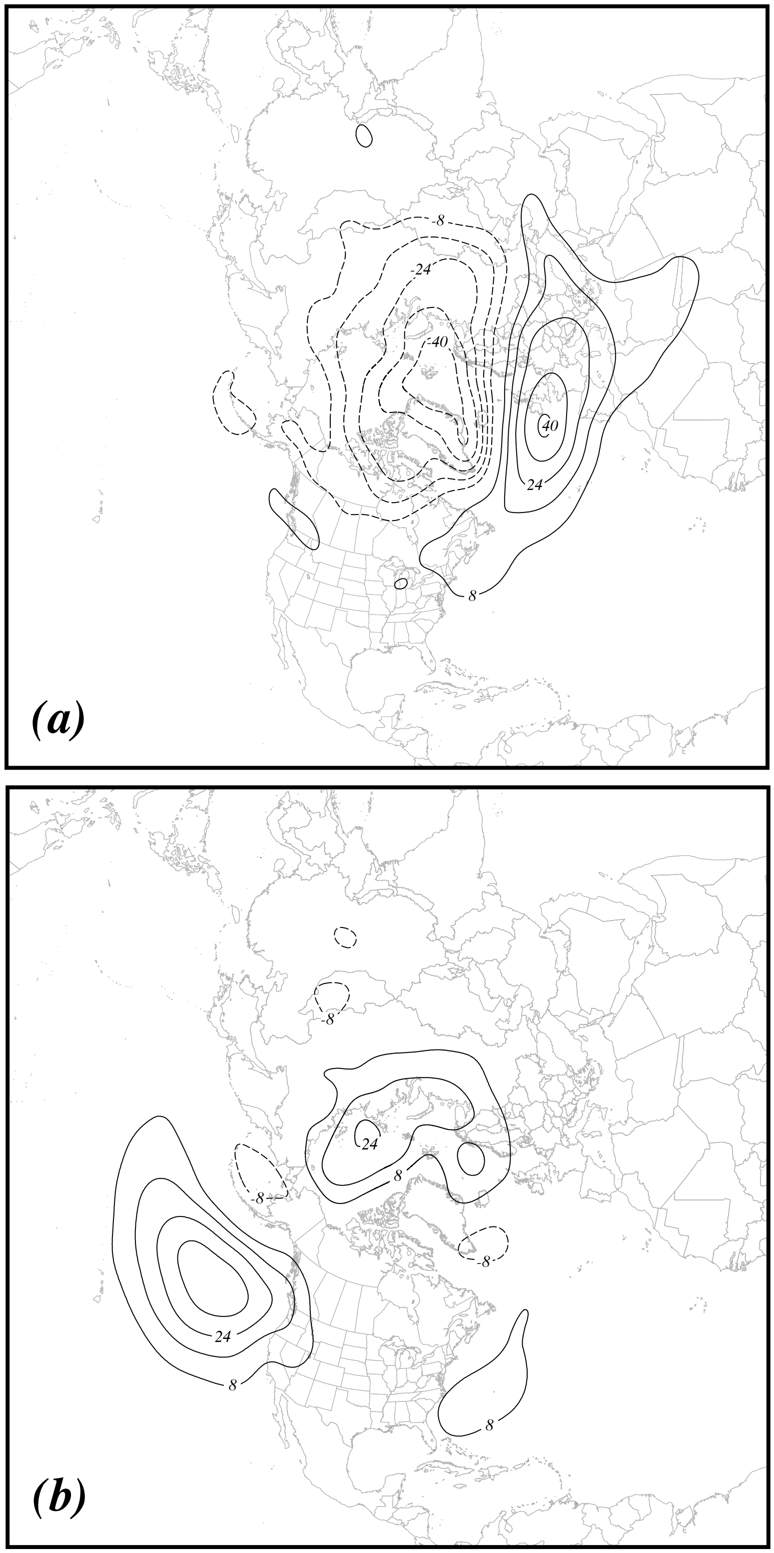


Fig. 10. 1000 hPa height differences between composite waviest and least wavy (a) polar jet and (b) subtropical jet seasons. See text for explanation and identification of the specific years comprising each composite. Positive (negative) height differences are in solid (dashed) lines, labeled in m and contoured every 8m (-8m) beginning at 8m (-8m).

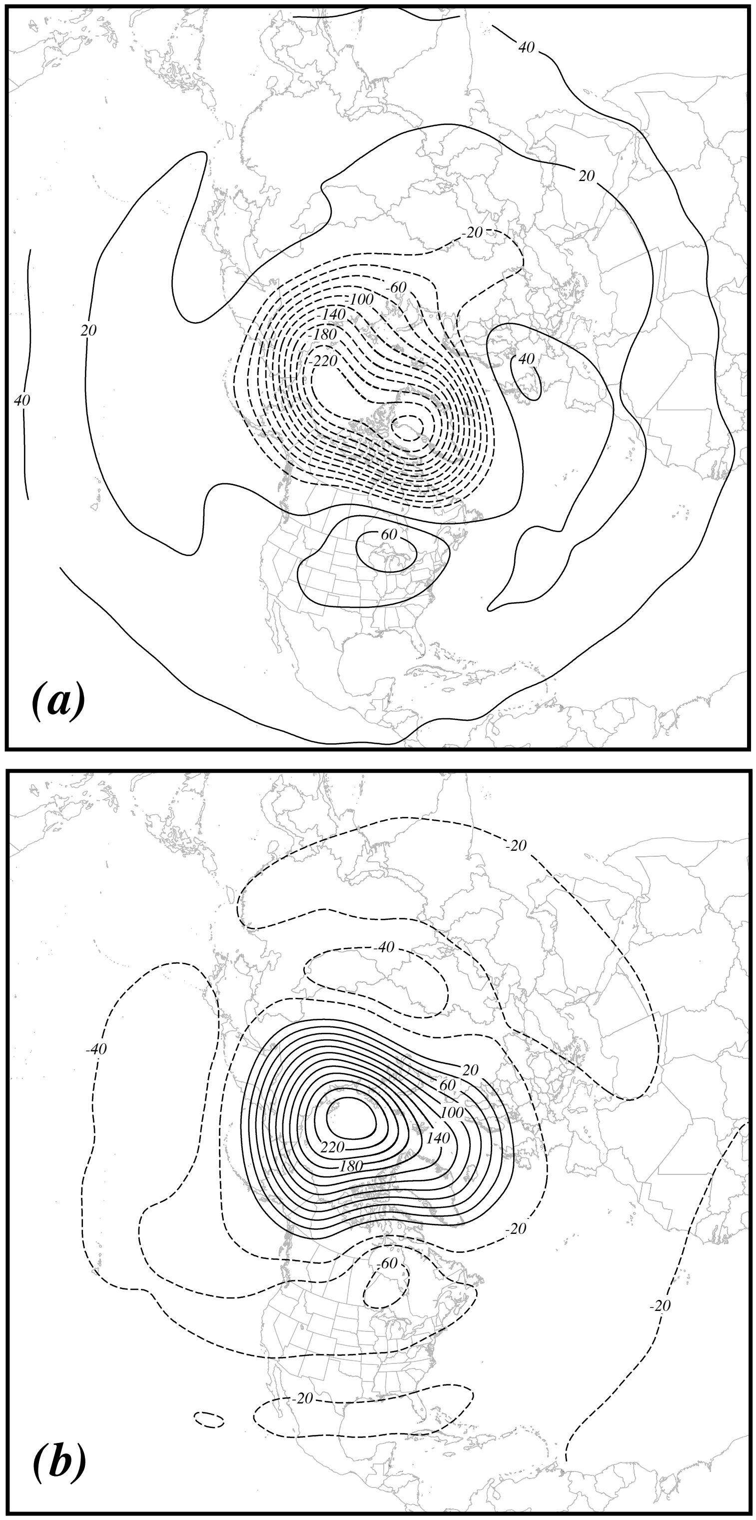


Fig. 11. 50 hPa height differences between composite waviest and least wavy (a) polar jet and (b) subtropical jet seasons. See text for explanation and identification of the specific years comprising each composite. Positive (negative) height differences are in solid (dashed) lines, labeled in m and contoured every 20m (-20m) beginning at 20m (-20m).